Street map analysis with excitable chemical medium

Andrew Adamatzky,[*] Neil Phillips,[†] Roshan Weerasekera,[‡] and Michail-Antisthenis Tsompanas[§]
Unconventional Computing Laboratory, University of the West of England, Bristol, United Kingdom

Georgios Ch. Sirakoulis[‖]
Department of Electrical and Computer Engineering, Democritus University of Thrace, Xanthi, Greece

(Received 5 March 2018; revised manuscript received 3 June 2018; published 13 July 2018)

Belousov-Zhabotinsky (BZ) thin layer solution is a fruitful substrate for designing unconventional computing devices. A range of logical circuits, wet electronic devices, and neuromorphic prototypes have been constructed. Information processing in BZ computing devices is based on interaction of oxidation (excitation) wave fronts. Dynamics of the wave fronts propagation is programed by geometrical constraints and interaction of colliding wave fronts is tuned by illumination. We apply the principles of BZ computing to explore a geometry of street networks. We use two-variable Oregonator equations, the most widely accepted and verified in laboratory experiments BZ models, to study propagation of excitation wave fronts for a range of excitability parameters, with gradual transition from excitable to subexcitable to nonexcitable. We demonstrate a pruning strategy adopted by the medium with decreasing excitability when wider and ballistically appropriate streets are selected. We explain mechanics of streets selection and pruning. The results of the paper will be used in future studies of studying dynamics of cities and characterizing geometry of street networks.

DOI: 10.1103/PhysRevE.98.012306

I. INTRODUCTION

Cities are often seen as spatially extended nonlinear systems in terms of their space-time dynamics of vehicular and pedestrian traffic: cities grow similarly to diffusion-limited aggregation, breath, and pulsate [1–6]. Social and physical processes—waves of traffic jams [7–13] and excitation, contagion, and diffusion of riots [14,15]—emerging on city streets often resemble excitation waves in chemical media [16,17]. To advance this analogy we consider that city streets are filled with an excitable chemical system—the Belousov-Zhabotinsky (BZ) medium [18,19]—and study space-time dynamics of traversing the street network with oxidation wave fronts for a range of light-controlled excitability parameters.

A thin-layer BZ medium shows rich dynamics of excitation waves, including target waves, spiral waves, and localized wave fragments and their combinations. A substantial number of theoretical and experimental laboratory prototypes of computing devices made of BZ medium has been reported in the last 30 years. Most interesting include logical gates implemented in geometrically constrained BZ medium [20,21], memory in BZ microemulsion [22], information coding with frequency of oscillations [23], chemical diodes [24], neuromorphic architectures [25–29], associative memory [30,31], wave-based counters [32], evolving logical gates [33], and binary arithmetic circuits [34–38]. By controlling BZ medium excitablity we can produce related analogs of dendritic trees [27], polymorphic logical gates [39], and logical circuits [40]. Light-sensitive modification, with $Ru(bpy)_2^{+3}$ as catalyst, allows for manipulation of the medium excitablity and subsequent modification of geometry of excitation wave fronts [41–43]. A light-sensitive BZ medium allows for optical inputs of information as parallel inputs in massive parallel processors. The medium can be also constrained geometrically in networks of conductive channels, thus allowing for a directed routing of signals.

We simulate light-sensitive BZ medium using two-variable Oregonator model [44] adapted to a light-sensitive BZ reaction with applied illumination [45].

The Oregonator equations in nonlinear chemistry are as important as, and phenomenologically equivalent to, Hodgkin-Huxley [46] and FitzHugh-Nagumo [47,48] equations in neurophysiology, Brusselator [49] in thermodynamics, Meinhardt-Gierer [50] in biology, Lotka-Volterra [51,52] in ecology, and the Fisher equation in genetics [53]. The Oregonator equations are proven to adequately reflect behavior of real BZ media in laboratory conditions, including triggers of excitation waves in three dimensions [54], phenomenology of excitation patterns in a medium with global negative feedback [55], controlling excitation with direct current fields [56], dispersion of periodic waves [57], three-dimensional scroll waves [58], and excitation spiral breakup [59]. Authors of present paper employed the Oregonator model as a virtual test bed in designing BZ medium-based computing devices which were implemented experimentally [33,40,60–63]. Therefore the Oregonator model is proven to be an adequate computational substitute of laboratory experiments.

Approximation of the shortest path, also in the context of the maze-solving problem, with BZ was studied experimentally in

[*]andrew.adamatzky@uwe.ac.uk
[†]neil.phillips@uwe.ac.uk
[‡]roshan.weerasekera@uwe.ac.uk
[§]antisthenis.tsompanas@uwe.ac.uk
[‖]gsirak@ee.duth.gr

Refs. [64–66], approximation of distance fields used in robot navigation [67], and partly applied in on-board controllers for robots [68,69]. All previous theoretical and experimental works on space exploration with the BZ medium dealt with the medium in excitable model. When exploring a geometrically constrained space filled with excitable BZ medium excitation wave fronts typically propagate in all directions, exploring all possible channels, as a flood fills. Excitation waves in subexcitable medium behave sometimes as localized patterns, quasidissipative solitons, and, thus, they might not explore all space available [61,70,71].

The paper is structured as follows. We introduce the Oregonator model of a light-sensitive BZ reaction and other components of modeling in Sec. II. We exemplify and discuss spatial dynamics of excitation on a London streets template in Sec. III. We uncover mechanisms of streets spanning by wave of excitation and analyze ballistic properties of wave fragments in subexcitable BZ medium in Sec. IV. We discuss outcomes of the study in Sec. V.

II. METHODS

A fragment of a London street map (map data ©2018 Google) approximately 2 km by 2 km, centered around London Bridge, was mapped onto a grid of 2205 by 2183 nodes (Fig. 1). Nodes of the grid corresponding to streets are considered to be filled with BZ medium, i.e., excitable nodes, other nodes are nonexcitable (Dirichlet boundary conditions, where the value of variables is fixed zero). We use two-variable Oregonator equations [44] adapted to a light-sensitive BZ reaction with applied illumination [45]:

$$\frac{\partial u}{\partial t} = \frac{1}{\epsilon}\left(u - u^2 - (fv + \phi)\frac{u - q}{u + q}\right) + D_u \nabla^2 u,$$
$$\frac{\partial v}{\partial t} = u - v. \qquad (1)$$

The variables u and v represent local concentrations of an activator, or an excitatory component of BZ system, and an inhibitor, or a refractory component. Parameter ϵ sets up a ratio of timescale of variables u and v, q is a scaling parameter depending on rates of activation or propagation and inhibition, and f is a stoichiometric coefficient. Constant ϕ is a rate of inhibitor production. In a light-sensitive BZ ϕ represents the rate of inhibitor production proportional to intensity of illumination. The parameter ϕ characterizes excitability of the simulated medium. The larger ϕ the less excitable medium is. We integrated the system using the Euler method with five-node Laplace operator, time step $\Delta t = 0.001$, and grid point spacing $\Delta x = 0.25$, $\epsilon = 0.02$, $f = 1.4$, $q = 0.002$. We varied the value of ϕ from the interval $\Phi = [0.05, 0.08]$. The model has been verified by us in experimental laboratory studies of the BZ system, and the sufficiently satisfactory match between the model and the experiments was demonstrated in Refs. [60–63]. To generate excitation wave fragments we perturb the medium by a square solid domains of excitation, 20×20 sites in state $u = 1.0$. Time-lapse snapshots provided in the paper were recorded at every 150th time step, and we display sites with $u > 0.04$; videos supplementing figures were produced by saving a frame of the simulation every 50th step of numerical integration and assembling them in the video with play rate 30 fps. All figures in this paper show time-lapse snapshots of waves, initiated just once from a single source of stimulation; these are not trains of waves following each other.

(a)

(b)

FIG. 1. Fragment of London street map used in computational experiments. Position of initial excitation is shown by "S" in the top of the North-West quadrant. (a) Google map, ©2018 Google [72]. (b) Template used for studies.

III. DYNAMICS OF EXCITATION

An excitable medium with values of ϕ from the lower end of interval Φ exhibits excitation waves propagating along all streets, independent on their width, and passes a junction where streets join each at various angles [Fig. 2(a)]. The excitation disappears when all waves reach boundaries of the

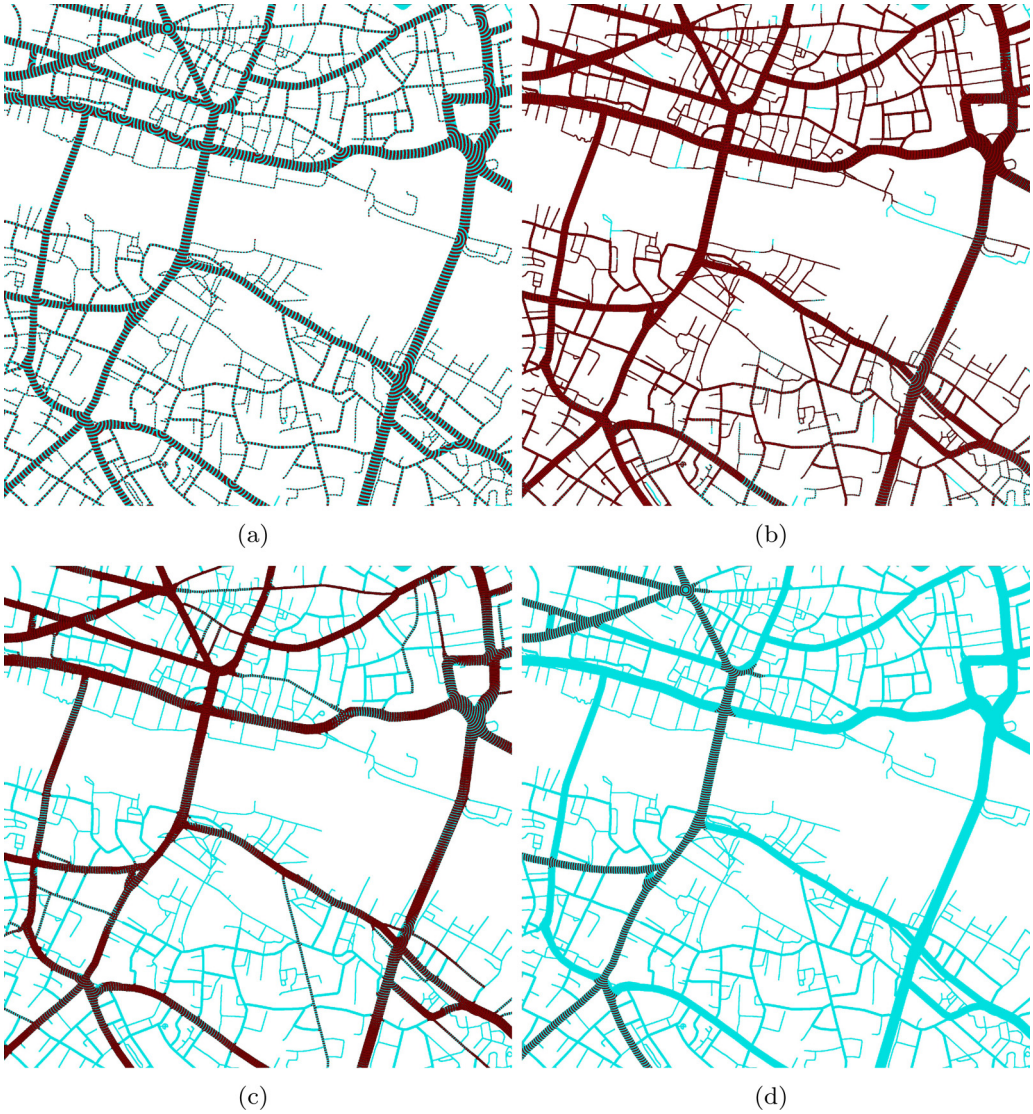

FIG. 2. Propagation of excitation on the street map for (a) $\phi = 0.055$, (b) $\phi = 0.065$, (c) $\phi = 0.075$, (d) $\phi = 0.078$. These are time-lapse snapshots of a single wave fragment recorded every 150th step of numerical integration. See videos in [73].

map. Integral dynamics of excitation is characterized by a sharp increase in a number of excited nodes followed by abrupt disappearance of the excitation when all wave fronts leave the lattice (e.g., Fig. 3, $\phi = 0.052$).

With an increase of ϕ to the middle of Φ we observe repeated propagation of excitation wave fronts along some parts of the map. Paths of the streets where excitation cycles are seen as having higher density of wave fronts are shown in Fig. 2(b). Two peaks in the excitation activity seen in the plot $\phi = 0.065$ (Fig. 3) are due to a combination of two factors: structure of the street network and cycles of excitation emerged. The street map graph consists of Northern and Southern parts connected by few bridges over the Thames. The medium is excited in its northernmost part domain of the street map (Fig. 1). Therefore, by the time excitation wave fronts cross bridges into the Southern part, the excitation propagates along all streets in the Northern part and disappear across the borders of the integration grid. When excitation in the Northern part disappears, just after the 20 000th step of integration, we observe a sudden drop in the number of excited nodes. The streets in the Southern part are then getting excited.

The value $\phi = 0.064$ is the highest for which all streets are covered by excitation wave fronts (Fig. 4). For $\phi = 0.075$ excitation waves propagate only along major streets [Fig. 2(c)]. And just few of the major streets are selected by excitation for $\phi = 0.078$ [Fig. 2(d)]. Due to excitation following only selected paths an overall time the medium stays excited becomes substantial, up to 100 000 iterations (Fig. 3).

Spatial coverage of street networks by excitation wave fronts for various values of ϕ is decreasing with the decrease of the medium's excitability (increase of ϕ), as illustrated in Fig. 5. Looking at Fig. 5 one might think that by decreasing excitability we prune the street network by selecting only widest streets. This is partly but not always true. The explanations are in the next section.

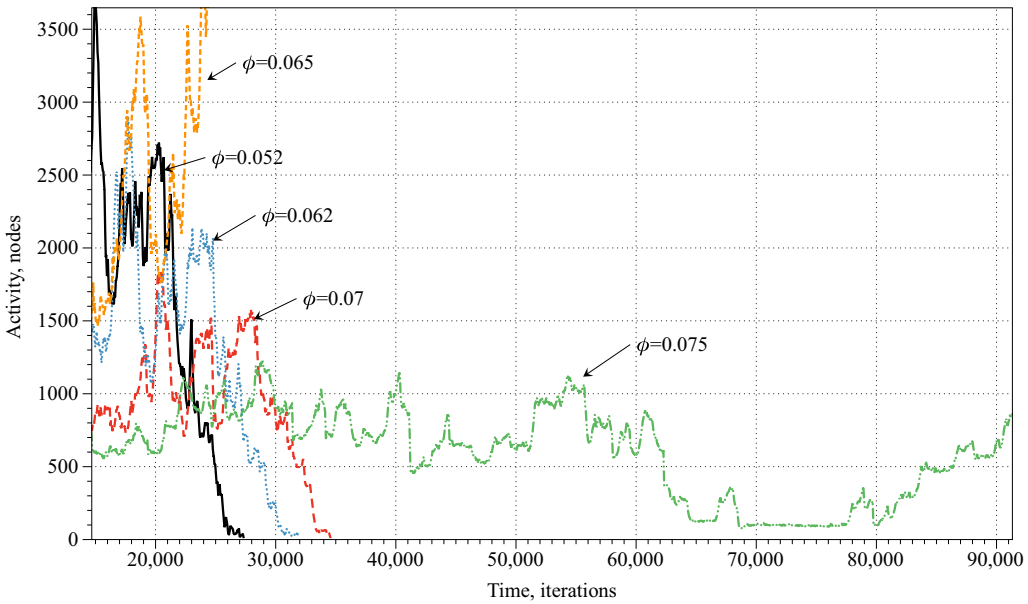

FIG. 3. Integral dynamics of excitation calculated as a number of grid nodes with $u > 0.1$ at each time step of integration. The dynamics is shown for the media with $\phi = 0.052, 0.062, 0.065, 0.07, 0.075$. The dynamics is show till the moment when excitation waves disappear or all streets got covered, whichever occurs earlier. Data are available in [73].

IV. MECHANICS OF EXPLORATION

Dynamical regimes of BZ medium can be subdivided to excitable $\phi < 0.064$, subexcitable $0.064 \leqslant \phi < 0.08$ and nonexcitable $0.08 \leqslant \phi$. In excitable mode a perturbation leads to formation of circular wave fronts [Fig. 6(a)], which propagates in all directions. If streets are filled with excitable medium, then, independently of a site of initial perturbation excitation travels to all streets. In a subexcitable medium we can observe three regimes of the medium response to asymmetric perturbation: expanding wave fronts, $0.0766 \leqslant \phi \leqslant 0.076690$ [Fig. 6(b)], shape-preserving wave fronts, $0.076691 \leqslant \phi \leqslant 0.076698$ [Fig. 6(c)], and collapsing wave fronts, $0.076691 \leqslant \phi \leqslant 0.076699$ [Fig. 6(d)].

Proposition 1. A coverage of a street network by an excitation originated in an arbitrary point of the street network filled with BZ medium with $0.076 \leqslant \phi \geqslant 0.079$ is proportional to a ratio of junctions with street branching at acute angles met by propagating wave fronts.

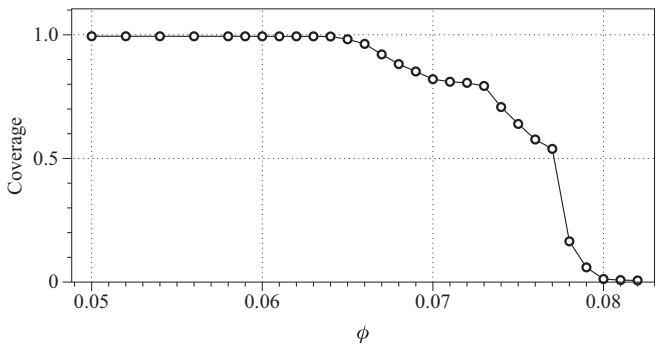

FIG. 4. Coverage of the street network by excitation waves for $\phi \in \Phi$. A value of coverage is calculated as a ratio of nodes, representing streets, excited ($u > 0.1$) at least once during the medium's evolution to a total number of nodes representing streets. Values of coverage are displayed by circles for ϕ increasing from 0.05 with increment 0.001.

Formal proof of this proposition will be the scope of future studies. Here we consider constructive support of the statement. All three types of subexcitable waves propagate alike at the initial stages of their evolution: they preserve their shape and velocity vector. When such waves collide into nonexcitable object they do not reflect but partly annihilate. If—depending on an angle of collision—some part of the wave front did not come in contact with nonexcitable object it might restore its shape, especially if the medium is in the expanding wave mode, and continue its propagation. Shape preservation and ballistic propagation of wave fragments in subexcitable medium for higher values of ϕ ($\phi \geqslant 0.076$) prevent excitation from entering site streets. Chances that a wave front enters a side street are proportional to the angle between wave-front velocity vector and a vector from the main street to the side street. This is illustrated in Fig. 7. Coverage versus ϕ plots for street network Fig. 1 and test structure Fig. 7 are shown in Fig. 8. Linear fits of the plots are as follow: $\text{coverage}_{\text{street}} = -63.994\phi + 5.4507$ and $\text{coverage}_{\text{test}} = -187.5\phi + 14.713$. The test structure Fig. 7 has equal numbers of junctions with acute and obtuse angles. Absolute value of the slop of $\text{coverage}_{\text{street}}$ is lower than that of the slop of $\text{coverage}_{\text{test}}$. This might indicate that an excitation wave fronts propagating from the chosen site of perturbation (labeled by "s" in Fig. 1) encounter more junctions with acute angles. Indeed, we could expect different slope of a coverage for another site of initial perturbation that would be a matter of further studies.

A network of channels filled with BZ medium is commutative if the following condition takes place: if an excitation wave front originated by a perturbation of site a reaches site b then the excitation wave front originated by a perturbation of site b reaches site a. If BZ medium is in its excitable mode then the network is commutative. To check if the same holds

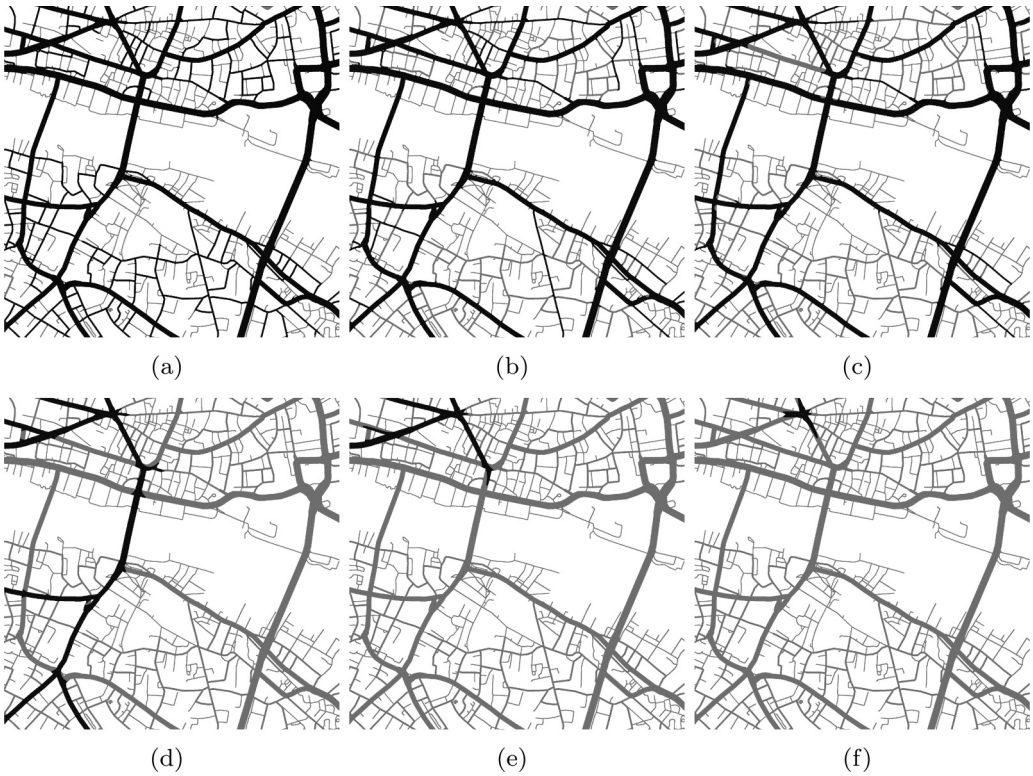

FIG. 5. Spatial coverage of street networks by excitation wave fronts for ϕ from (a) 0.072, (b) 0.075, (c) 0.076, (d) 0.078, (e) 0.079, (f) 0.080. Nodes, representing streets, which have been excited at least once during the medium evolution are black. Nodes which never been excited are light gray. Data are available in [73].

for subexcitable BZ medium we constructed a template of three channels shown in Fig. 9. We found that the template is commutative. A graph of reachability though is pruned with increase of ϕ. The graph [Fig. 9(e)] is fully connected in excitable medium, $\phi = 0.06$ [Figs. 9(a)–9(d)], tree [Fig. 9(j)] is obtained for $\phi = 0.0767$ [Figs. 9(f)–9(i)], chain and one isolated node [Fig. 9(o)] for $\phi = 0.078$ [Figs. 9(k)–9(n)], and a single edge and two isolated nodes [Fig. 9(t)] is the result for $\phi = 0.079$ [Figs. 9(p)–9(s)]. There is always a chance that we missed some configuration of channels which demonstrates noncommutativity for some values ϕ.

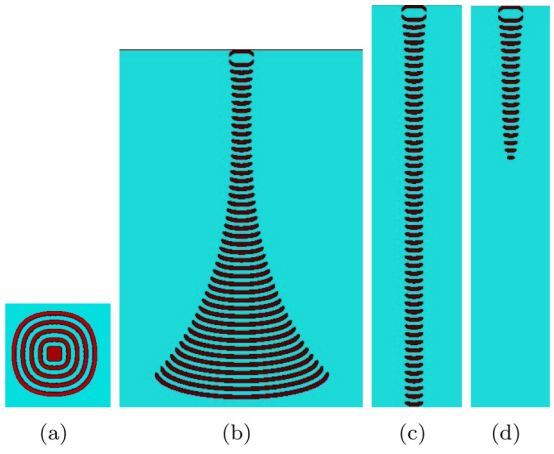

FIG. 6. Types of waves. All site of the medium are conducive for excitation. (a) Classical wave in an excitable medium, $\phi = 0.05$. (b), (c), (d) Behavior of an initially asymmetric excitation in BZ medium for different levels of excitability. (b) Expanding wave fragment, $\phi = 0.076690$, (c) shape-preserving wave fragment, $\phi = 0.076691$, (d) collapsing wave fragment, $\phi = 0.076699$. These are time-lapse snapshots of a single wave fragment recorded every 150th step of numerical integration.

V. DISCUSSION

Using numerical integration of the Oregonator model of Belousov-Zhabotinsky medium in a fragment of a London street network we demonstrated that (1) coverage of the network is proportional to excitability of the medium, (2) cycling patterns of excitation are only possible in the subexcitable regime of the medium, (3) wave fragments in a subexcitable network propagate ballistically, (4) coverage of the street network by excitation in a medium with a given value ϕ is proportional to a ratio of junctions with streets branching out at an acute angle to junctions with streets branching out at obtuse angles, and (5) reachability by excitation wave fronts is commutative.

Excitation wave fragments propagate ballistically. Close analogies could be a crowd charging along the streets or fluid jet streams propagating along the streets. To evaluate the analogy with a fluid flow we simulate jet streams entering streets from the Western edge of the street map domain and leaving in all other edges. We compared the dynamics of fluid flow with dynamics of excitation waves initiated at the Western edge of the integration grid. There is nearly a perfect match between fluid flow for Reynolds number Re = 1000 [Fig. 10(a)] and subexcitable medium with $\phi = 0.0767$ [Fig. 10(c)], with just

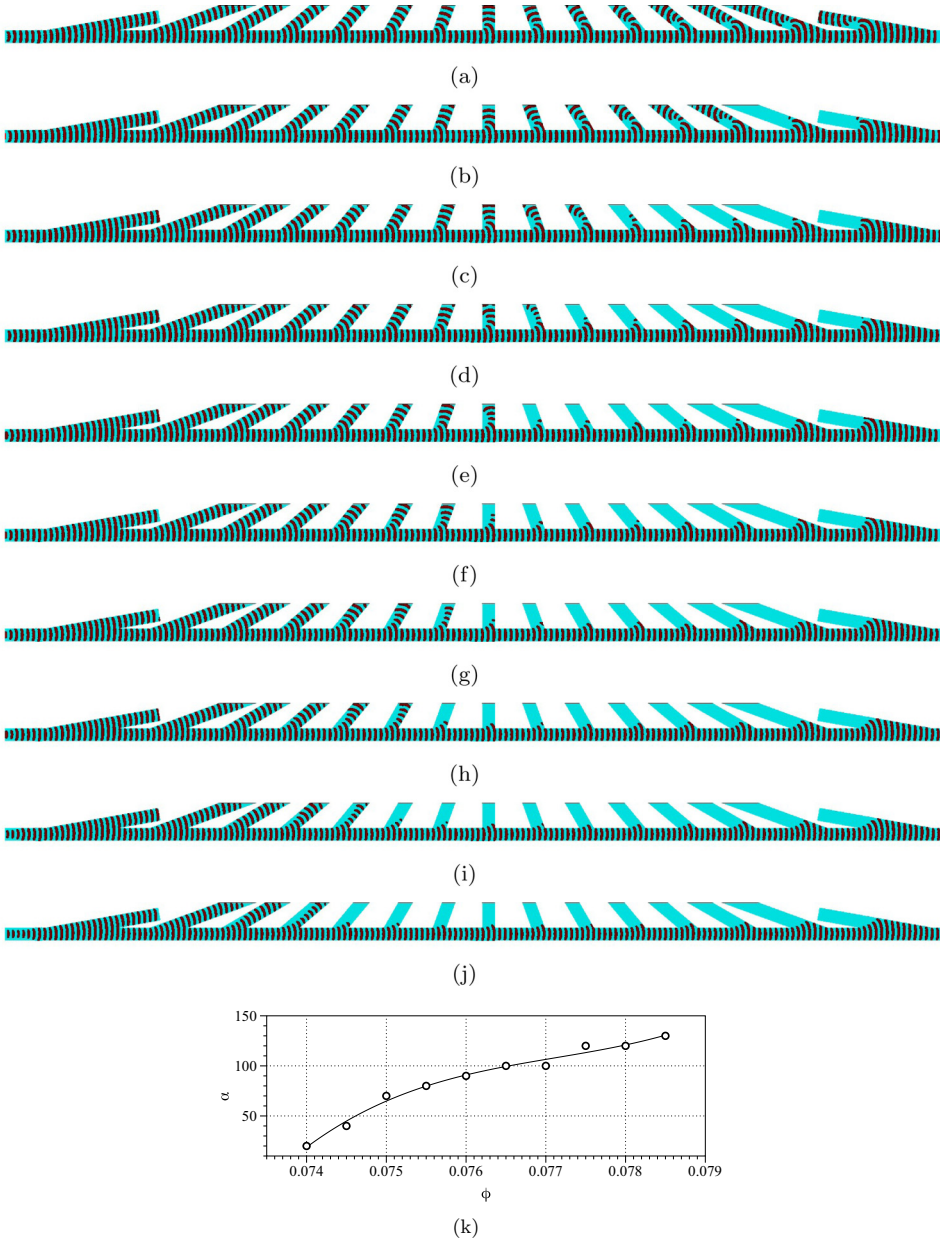

(k)

FIG. 7. Wave propagation to side channel depends on the medium's excitability (a)–(j) Excitation is initiated at the West top of the vertical channel. Side channels join the vertical channel at angles $\alpha = 20^o$ to 160^o with increment 10^o. These are time-lapse snapshots of a single wave fragment recorded every 150th step of numerical integration. Values of ϕ are (a) 0.07, (b) 0.071, (c) 0.072, (d) 0.073, (e) 0.074, (f) 0.075, (g) 0.076, (h) 0.077, (i) 0.078, (j) 0.079. (k) Minimal angles α of side channels occupied by excitation waves for $\phi = 0.074$ with increment 0.0005. Cubic fit $\alpha = (-720792) + 2.8017 \times 10^7\phi + (-3.6312 \times 10^8)\phi^2 + 1.5695 \times 10^9\phi^3$ is shown by line.

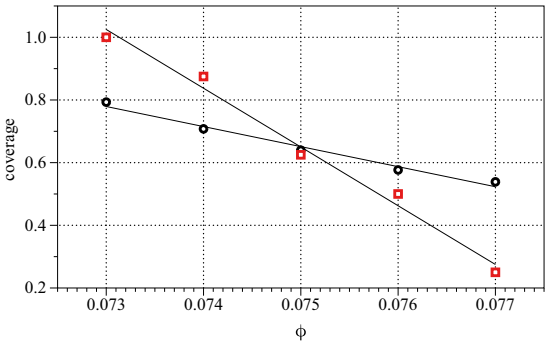

FIG. 8. Coverage of London street network, Fig. 1, black circles, and structure with equal number of acute and obtuse junctions, Fig. 7, red squares, by excitation waves in BZ medium with $\phi = 0.073$ to 0.077. Lines are linear fits: coverage of street map $5.4507 + (-63.994)\phi$ of test template, Fig. 7, $14.713 + (-187.5)\phi$.

one street (top of the North-West quadrant) covered by the a jet stream and not covered by excitation wave. Increase of Reynolds number leads to the effect of street pruning as occurs with increase of ϕ [Figs. 10(b) and 10(d)]; however, the coverage of streets by excitation waves is substantially different from that by fluid flow: the only match in the two streets in the South-West quadrant where flow is disrupted by turbulence [blue in Fig. 10(b)] and no excitation is traveling the same streets [Fig. 10(d)].

Ballistic behavior of the excitation-wave fragments is somewhat similar to herding behavior of crowds observed during various scenarios of evacuation, especially when stress is involved [74–77]. The herding behavior might lead to situations when a panic-stricken crowd traps itself in potentially dangerous domains of the space [78,79]. Exploring geometries with subexcitable medium could help us to identify loci of the space when a crowd charging in a herding mode could find itself stuck. Pruning behavior subexcitable BZ medium

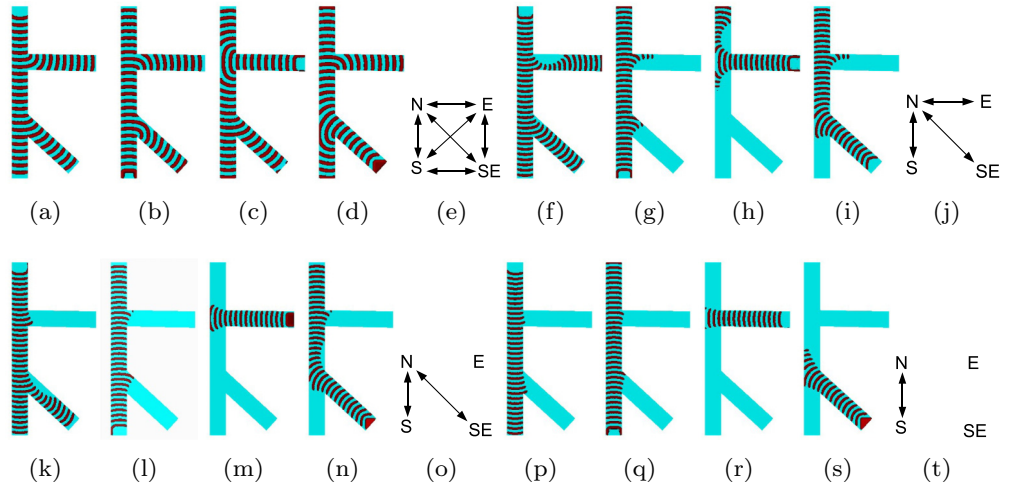

FIG. 9. Time-lapse snapshots of excitation waves initiated at end of North, "N," segment (a), (f), (k), (p); South, "S," segment (b), (g), (l), (q); East, "E," (c), (h), (m), (r); Southeast, "SE" (d), (i), (n), (s). Values of ϕ are as follows: (a–e) 0.06, (f–j) 0.0767, (k–o) 0.078, (p–t) 0.079. These are time-lapse snapshots of a single wave fragment recorded every 150th step of numerical integration.

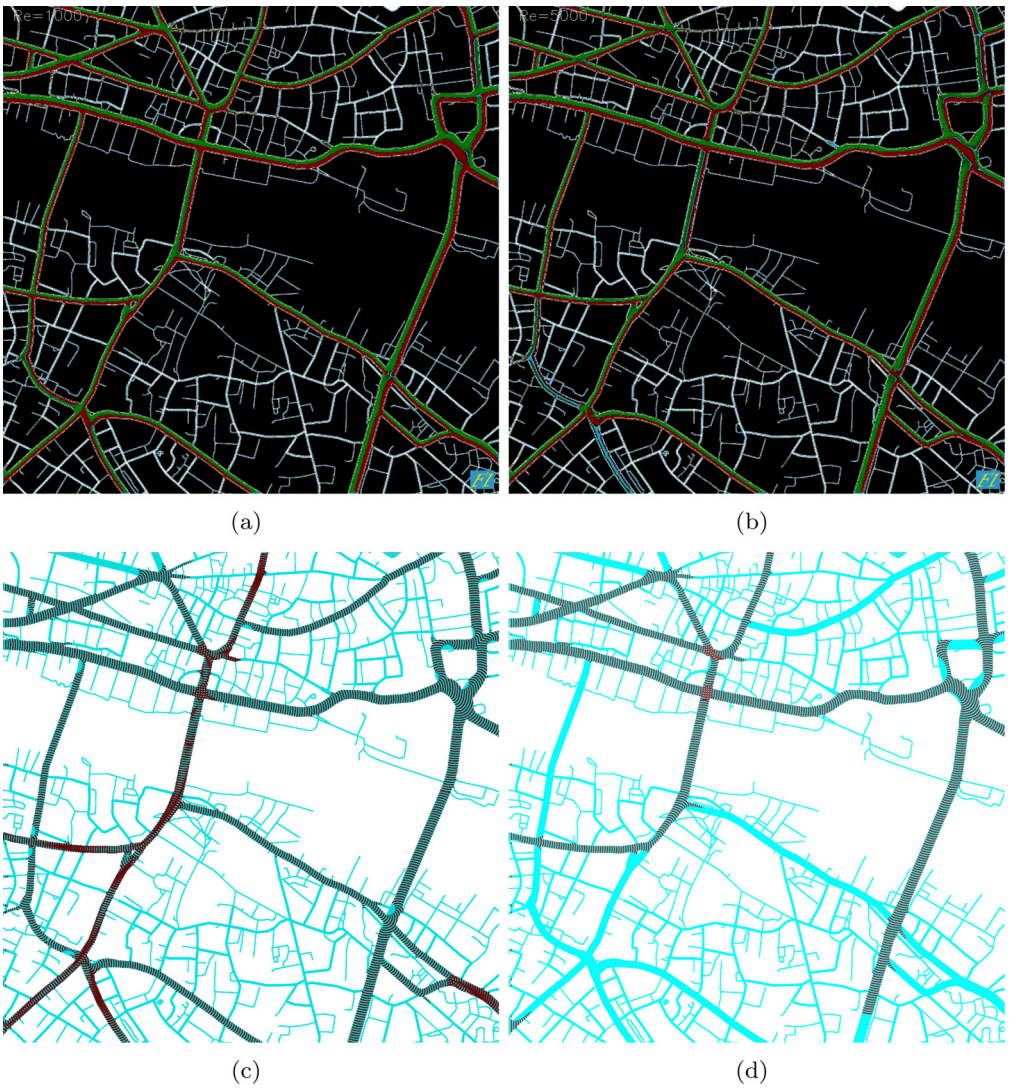

FIG. 10. Comparison of laminar fluid flow for (a) low Reynolds number Re = 1000 and (b) high Reynolds number Re = 5000 with excitation propagation for (c) $\phi = 0.0767$ and (d) $\phi = 0.078$. Fluid stream and excitation enter street networks at streets on the Northern edge. (a), (b) Snapshots of fluid streaming along streets produced in Fluid Flow Illustrator [80]. (c), (d) Time-lapse snapshots of wave fragments recorded every 150th step of numerical integration.

for high values of ϕ might also help to assess areas of a geometric network which would more frequently to be visited by living creature: this is based on our previous studies of space exploration by leeches [81,82].

[1] L. M. Bettencourt, J. Lobo, D. Helbing, C. Kühnert, and G. B. West, Proc. Natl. Acad. Sci. USA **104**, 7301 (2007).
[2] S. Hinchliffe and S. Whatmore, Sci Culture **15**, 123 (2006).
[3] L. Bettencourt and G. West, Nature (London) **467**, 912 (2010).
[4] M. Batty and S. Marshall, Town Planning Rev. **80**, 551 (2009).
[5] W. E. Rees, in *Sustainability Science* (Springer, New York, 2012), pp. 247–273.
[6] E. Flynn, Architec. Res. Q. **20**, 20 (2016).
[7] J. Long, Z. Gao, X. Zhao, A. Lian, and P. Orenstein, Netw. Spatial Econ. **11**, 43 (2011).
[8] J. A. Laval and L. Leclercq, Phil. Trans. R. S. Lond. A **368**, 4519 (2010).
[9] T. Nagatani, Phys. Rev. E **61**, 3564 (2000).
[10] T. Nagatani, Phys. Rev. E **59**, 4857 (1999).
[11] Z.-P. Li and Y.-C. Liu, Eur. Phys. J. B **53**, 367 (2006).
[12] Y. Jiang, R. Kang, D. Li, S. Guo, and S. Havlin, arXiv:1705.08269.
[13] D.-H. Sun, G. Zhang, M. Zhao, S.-L. Cheng, and J.-D. Cao, Comm. Nonlin. Sci. Numer. Sim. **56**, 287 (2018).
[14] M. Potegal and J. F. Knutson (eds.), The Dynamics of Aggression: Biological and Social Processes in Dyads and Groups (Lawrence Erlbaum Associates Hillsdale, New Jersey, 1994).
[15] D. J. Myers, Am. J. Sociol. **106**, 173 (2000).
[16] J. J. Tyson and J. P. Keener, Physica D **32**, 327 (1988).
[17] P. Jung, A. Cornell-Bell, F. Moss, S. Kadar, J. Wang, and K. Showalter, Chaos **8**, 567 (1998).
[18] B. P. Belousov, Compilation of Abstracts on Radiation Medicine **147**, 1 (1959) (in Russian).
[19] A. Zhabotinsky, Biofizika **9**, 11 (1964).
[20] O. Steinbock, P. Kettunen, and K. Showalter, J. Phys. Chem. **100**, 18970 (1996).
[21] J. Sielewiesiuk and J. Górecki, J. Phys. Chem. A **105**, 8189 (2001).
[22] A. Kaminaga, V. K. Vanag, and I. R. Epstein, Angew. Chem., Intl. Ed. **45**, 3087 (2006).
[23] J. Gorecki, J. N. Gorecka, and A. Adamatzky, Phys. Rev. E **89**, 042910 (2014).
[24] Y. Igarashi and J. Gorecki, Intl. J. Unconventional Comput. **7**, 141 (2011).
[25] J. Gorecki and J. N. Gorecka, Intl. J. Unconventional Comput. **2**, 321 (2006).
[26] P. L. Gentili, V. Horvath, V. K. Vanag, and I. R. Epstein, Intl. J. Unconventional Comput. **8**, 177 (2012).
[27] H. Takigawa-Imamura and I. N. Motoike, Neural Netw. **24**, 1143 (2011).
[28] J. Stovold and S. O'Keefe, in *International Conference on Information Processing in Cells and Tissues* (Springer, New York, 2012), pp. 143–149.
[29] G. Gruenert, K. Gizynski, G. Escuela, B. Ibrahim, J. Gorecki, and P. Dittrich, Intl. J. Neural Syst. **25**, 1450032 (2015).
[30] J. Stovold and S. O'Keefe, Intl. J. Parallel Emergent Distrib. Syst. **32**, 74 (2016).
[31] J. Stovold and S. O'Keefe, in *Advances in Unconventional Computing* (Springer, New York, 2017), pp. 141–166.
[32] J. Gorecki, K. Yoshikawa, and Y. Igarashi, J. Phys. Chem. A **107**, 1664 (2003).
[33] R. Toth, C. Stone, A. Adamatzky, B. de Lacy Costello, and L. Bull, Chaos Solitons Fractals **41**, 1605 (2009).
[34] B. D. L. Costello, A. Adamatzky, I. Jahan, and L. Zhang, Chem. Phys. **381**, 88 (2011).
[35] M.-Z. Sun and X. Zhao, J. Chem. Phys. **138**, 114106 (2013).
[36] G.-M. Zhang, I. Wong, M.-T. Chou, and X. Zhao, J. Chem. Phys. **136**, 164108 (2012).
[37] M.-Z. Sun and X. Zhao, Intl. J. Unconventional Comput. **11**, 165 (2015).
[38] S. Guo, M.-Z. Sun, and X. Han, Intl. J. Unconventional Comput. **11**, 131 (2015).
[39] A. Adamatzky, B. de Lacy Costello, and L. Bull, Intl. J. Bifurcation Chaos **21**, 1977 (2011).
[40] W. M. Stevens, A. Adamatzky, I. Jahan, and B. de Lacy Costello, Phys. Rev. E **85**, 066129 (2012).
[41] L. Kuhnert, Nature (London) **319**, 393 (1986).
[42] M. Braune and H. Engel, Chem. Phys. Lett. **204**, 257 (1993).
[43] N. Manz, V. A. Davydov, V. S. Zykov, and S. C. Müller, Phys. Rev. E **66**, 036207 (2002).
[44] R. J. Field and R. M. Noyes, J. Chem. Phys. **60**, 1877 (1974).
[45] V. Beato and H. Engel, in *SPIE's First International Symposium on Fluctuations and Noise* (International Society for Optics and Photonics, Bellingham, Washington, 2003), pp. 353–362.
[46] A. L. Hodgkin and A. F. Huxley, J. Physiol. **117**, 500 (1952).
[47] R. FitzHugh, Bull. Math. Biophys. **17**, 257 (1955).
[48] J. Nagumo, S. Arimoto, and S. Yoshizawa, Proc. IRE **50**, 2061 (1962).
[49] B. Gray and L. Aarons, in *Faraday Symposia of the Chemical Society* (Royal Society of Chemistry, London, United Kingdom, 1974), Vol. 9, pp. 129–136.
[50] A. Gierer and H. Meinhardt, Kybernetik **12**, 30 (1972).
[51] A. J. Lotka, Proc. Natl. Acad. Sci. USA **6**, 410 (1920).
[52] V. Volterra, *Variazioni e fluttuazioni del numero d'individui in specie animali conviventi* (C. Ferrari, 1927).
[53] R. A. Fisher, Ann. Human Genet. **7**, 355 (1937).
[54] A. Azhand, J. F. Totz, and H. Engel, EPL (Europhys. Lett.) **108**, 10004 (2014).
[55] V. K. Vanag, A. M. Zhabotinsky, and I. R. Epstein, J. Phys. Chem. A **104**, 11566 (2000).
[56] H. Ševíková, I. Schreiber, and M. Marek, J. Phys. Chem. **100**, 19153 (1996).
[57] J. Dockery, J. P. Keener, and J. Tyson, Physica D **30**, 177 (1988).
[58] A. T. Winfree and W. Jahnke, J. Phys. Chem. **93**, 2823 (1989).
[59] J. Taboada, A. Munuzuri, V. Pérez-Muñuzuri, M. Gómez-Gesteira, and V. Pérez-Villar, Chaos **4**, 519 (1994).
[60] A. Adamatzky and B. de Lacy Costello, Chaos Solitons Fractals **34**, 307 (2007).
[61] B. de Lacy Costello, R. Toth, C. Stone, A. Adamatzky, and L. Bull, Phys. Rev. E **79**, 026114 (2009).
[62] R. Toth, C. Stone, B. de Lacy Costello, A. Adamatzky, and L. Bull, *Theoretical and Technological Advancements in Nanotechnology and Molecular Computation: Interdisciplinary Gains* (IGI Global, 2010), Chap. 11, pp. 162–175.

[63] A. Adamatzky, B. De Lacy Costello, L. Bull, and J. Holley, Isr. J. Chem. **51**, 56 (2011).
[64] K. Agladze, N. Magome, R. Aliev, T. Yamaguchi, and K. Yoshikawa, Physica D **106**, 247 (1997).
[65] O. Steinbock, Á. Tóth, and K. Showalter, Science **267**, 868 (1995).
[66] N. Rambidi and D. Yakovenchuck, BioSystems **51**, 67 (1999).
[67] A. Adamatzky and B. de Lacy Costello, Naturwissenschaften **89**, 474 (2002).
[68] A. Adamatzky, B. de Lacy Costello, C. Melhuish, and N. Ratcliffe, Materials Sci. Eng. C **24**, 541 (2004).
[69] A. Vázquez-Otero, J. Faigl, N. Duro, and R. Dormido, Intl. J. Unconventional Comput. **10**, 295 (2014).
[70] M. Hildebrand, H. Skødt, and K. Showalter, Phys. Rev. Lett. **87**, 088303 (2001).
[71] A. Adamatzky, Chaos Solitons Fractals **21**, 1259 (2004).
[72] https://www.google.co.uk/maps/search/london+bridge/@51.5072749,-0.0906453,15.75z.
[73] Exemplar videos of excitation wave fronts propagating on the London street network, time lapse images of excitations, images of coverage frequency, and logs of activity are available at Zenodo, doi: 10.5281/zenodo.1303882.
[74] X. Zheng, T. Zhong, and M. Liu, Building Environ. **44**, 437 (2009).
[75] M. Burger, P. Markowich, and J.-F. Pietschmann, Kinet. Relat. Models **4**, 1025 (2011).
[76] D. Helbing, I. Farkas, and T. Vicsek, Nature (London) **407**, 487 (2000).
[77] C. Vihas, I. Georgoudas, and G. C. Sirakoulis, J. Cellular Automata **8**, 333 (2013).
[78] D. Helbing, I. J. Farkas, P. Molnar, and T. Vicsek, Pedestrian and Evacuation Dynamics **21**, 21 (2002).
[79] D. Helbing, I. J. Farkas, and T. Vicsek, in *The Science of Disasters* (Springer, New York, 2002). pp. 330–350.
[80] http://www.flowillustrator.com/.
[81] A. Adamatzky, Biosystems **130**, 28 (2015).
[82] A. Adamatzky and G. C. Sirakoulis, Biosystems **134**, 48 (2015).